Alteration processes of mantle peridotite in the Samail ophiolite inferred from independent component analysis of rock physical properties

Y. Akamatsu[1*], T. Kuwatani[1], and R. Oyanagi[2,1]

1. Research Institute for Marine Geodynamics, Japan Agency for Marine–Earth Science and Technology (JAMSTEC), Kanagawa, Japan

2. School of Science and Engineering, Kokushikan University, Tokyo, Japan

*Corresponding author: Yuya Akamatsu (akamatsuy@jamstec.go.jp)

This is a non-peer reviewed preprint submitted to LITHOS.

Abstract

To quantify the alteration processes of mantle from geophysical data, an understanding of the relationship between alteration and the physical properties of mantle peridotite is essential. In this study, we employed independent component analysis (ICA) to evaluate variations in the physical properties of altered peridotites collected by the Oman Drilling Project, to understand the alteration processes of mantle peridotite in the Samail ophiolite. We analyzed multivariate physical properties (density, porosity, P-wave velocity, electrical resistivity, permeability, magnetic susceptibility, and color reflectance) that had been measured on core samples. The ICA results show that the observed variations in physical properties can be explained broadly by four independent components. Through their relationships with physical properties and comparisons with petrological and geochemical data from previous studies, we infer the four independent components to represent distinct alteration processes: the early and late stages of serpentinization, magnetite formation, and near-surface carbonation. These processes develop differently during the overall process of alteration, and they influenced each physical property in different ways. Our results demonstrate that ICA can separate the effects of multiple processes of alteration on various physical properties of the altered peridotites, which previously had been difficult to quantify.

Highlights

- ICA was used to evaluate mantle alteration processes in the Samail ophiolite
- We utilized data on the multivariate physical properties of drillcores
- Four independent components represent processes of serpentinization and carbonation

Keywords

serpentinization; mantle; physical property; independent component analysis; the Oman Drilling Project

1 Introduction

The alteration of mantle peridotite to serpentinite (i.e., serpentinization) is a crucial process in the geodynamic evolution of Earth, and it plays a significant role in various geological processes such as the tectonic evolution of slow-spreading ridges (e.g., Escartín et al., 1997), the triggering of intermediate-depth earthquakes at subduction zones (e.g., Ferrand et al., 2017; Peacock, 2001; Yoshida et al., 2023), the global water and carbon cycles (e.g., Hatakeyama et al., 2017; Katayama et al., 2023; Okamoto et al., 2021), and hydrogen production in the subsurface biosphere (e.g., Miller et al., 2016; Takai et al., 2006). Because serpentinization modifies the physical properties of peridotite, altered mantle can be identified as a geophysical anomaly in geophysical explorations, including seismological and electromagnetic surveys of the seafloor (Fujie et al., 2013; Grevemeyer et al., 2007; Muller et al., 1997; Okino et al., 2004; Ranero et al., 2003). To extract the data for each alteration process quantitatively by interpreting these geophysical data, a detailed understanding of the relationship between alteration and the physical properties of mantle peridotite is essential.

Serpentinization changes the seismic velocity of rock due to the weak elasticity of serpentine compared with olivine (Christensen, 2004), and serpentinization induces dilation that results in the development of cracks during the reaction (Macdonald and Fyfe, 1985). This is called reaction-induced cracking and results in drastic changes in the physical properties of mantle peridotite that are sensitive to porosity, such as seismic velocity, electrical resistivity, and permeability. The enhancement of permeability due to the reaction-induced cracking accelerates the reaction and promotes further infiltration of water, thereby resulting in self-promoting serpentinization within a positive feedback system (Jamtveit et al., 2008). Serpentinization also changes the magnetic and electrical properties of mantle peridotite due to the formation of magnetite via a series of reactions (Bach et al., 2006; Katayama et al., 2020; Kawano et al., 2012; Oufi et al., 2002; Toft et al., 1990).

Previous laboratory studies have investigated the relationships between alteration and the individual physical properties of mantle peridotite. However, alteration of mantle peridotite is a complex physicochemical process that involves various reactions and brittle fracturing, as described above. In addition, oceanic plates can undergo multiple stages of deformation and alteration in various environments, from their formation at a mid-ocean ridge to their subduction and/or exposure at the surface or seafloor, and mantle peridotites often record a history of multiple processes of alteration. It is difficult, therefore, to evaluate a series of alteration processes from a single physical property.

In this study, we performed multivariate analysis to integrate the various physical properties of altered mantle peridotite. Multivariate analysis is an analytical method that treats multidimensional data statistically to extract the essential dimensions related to the crucial processes that underlie the data, and various methods have been used for extracting geological processes from geoscientific data (Iwamori and Albarède, 2008; Kuwatani et al., 2014; Yoshida et al., 2018). We employed Independent Component Analysis (ICA), which separates a set of mixed signals into statistically independent components, thereby enabling the extraction of unique and distinct sources of data from complex datasets (Hyvärinen et al., 2001). ICA has been applied in the field of Earth sciences (e.g., using geochemical datasets) and it is now well-established as an analytical technique for extracting independent geological processes from multidimensional data (e.g., Iwamori et al., 2017; Iwamori and Albarède, 2008; Yasukawa et al., 2016). We employed, therefore, ICA to extract multiple processes involved in the alteration of mantle peridotite in the Samail ophiolite. We used samples that had been collected from the mantle section of the Samail ophiolite in Oman during the Oman Drilling Project. These rocks have undergone multiple stages of alteration, with the primary minerals, such as oilivine and pyroxene, being moderately to completely replaced with secondary alteration products, such as serpentine (Kelemen et al., 2021). Multiple physical properties were measured onboard the drilling vessel (D/V) *Chikyu* from discrete cubic samples of drillcore (Kelemen et al., 2020a, 2020b), and we subjected these measurements to multivariate analysis. The dataset obtained onboard included porosity, density, elastic wave velocity, electrical resistivity, permeability, magnetic susceptibility, and color reflectance. Using the data for these multidimensional physical properties, we were able to extract the various alteration processes that had affected the mantle peridotites.

2 Geological setting

The Samail ophiolite in the Sultanate of Oman and the United Arab Emirates is the most extensive and best-exposed cross-section of oceanic lithosphere (Fig. 1a), and it contains complete sections from sediments and pillow lava to mantle peridotite (Fig. 1b). The mantle section of the Samail ophiolite is composed mainly of harzburgite and dunite. Harzburgite is a remnant rock formed by the partial melting of mantle diapirs that rose rapidly in the deep part of a spreading ridge. Dunite is a reaction product of the partial melting of basaltic melt that reacts with ascending harzburgite to completely dissolve orthopyroxene (Kelemen et al., 1995). The mantle peridotite in the Samail ophiolite records multiple stages of hydration (serpentinization) during its geological history, including hydrothermal circulation close to a mid-ocean ridge, obduction, and ongoing weathering (Boudier et al., 2010; Kelemen et al., 2021). The ongoing weathering at the surface involves low-temperature carbonation of the altered peridotite, with minerals such as calcite and magnesite produced by the reaction of CO_2 with the peridotite (Kelemen and Matter, 2008).

To asses the nature of alteration processes recorded in the Samail ophiolite, continuous cores through the crustal section to the mantle section of the ophiolite were sampled recently with a recovery rate of ~100% during the Oman Drilling Project of the International Continental Drilling Program (ICDP) (Kelemen et al., 2020c). The recovered cores were loaded into the laboratory of the D/V *Chikyu*, and systematic and comprehensive descriptions and measurements were made onboard from various perspectives, such as igneous and alteration petrology, structural geology, geochemistry, paleomagnetism, and physical properties, based on the protocols of the International Oceanic Drilling Program (IODP) (Kelemen et al., 2020c).

3 Materials and methods

3.1 Core samples

The Oman Drilling Project obtained continuous core samples from the dike–gabbro transition to the uppermost mantle of the Samail ophiolite (Kelemen et al., 2020c). The present study considers core samples from Holes BA1B and BA4A. These cores were recovered

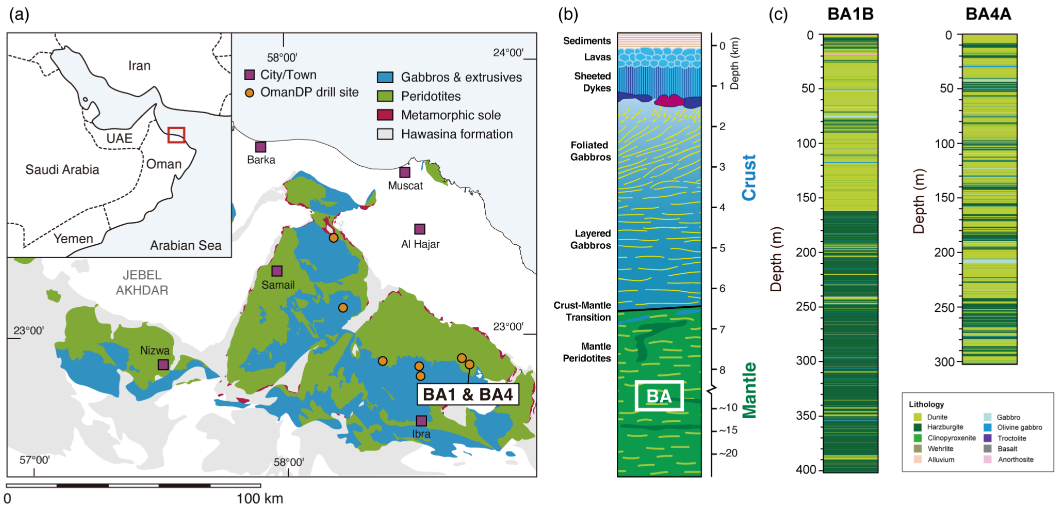

Fig. 1 (a) Geological map of the southeastern massif of the Samail ophiolite, modified after Kelemen et al. (2020c). The lithologies are based on Nicolas et al. (2000), and the locations of the Oman Drilling Project drill sites, including Holes BA1B and BA4A, are indicated. The colored units represent the ophiolite sequence. The inset shows the location of the main figure within the Arabian Peninsula. (b) Simplified stratigraphy of the Oman ophiolite. Holes BA1B and BA4A correspond to the mantle section. (c) Borehole stratigraphy of Holes BA1B and BA4A.

from the mantle section of the Samail ophiolite, and their lengths are respectively ~400 and ~300 meters (Fig. 1c). Hole BA1B sampled an upper dunite section that overlies a lower harzburgite section, whereas Hole BA4A sampled mainly dunite. Core samples from the mantle sections are highly altered and the dunite samples tend to be more altered than the harzburgites (Kelemen et al., 2021). The highly altered samples display a mesh texture, which is characteristic of low-temperature serpentinite. Details of the geology around the holes are provided by Kelemen et al. (2021).

3.2 Physical properties

The physical properties of the recovered core samples were measured systematically onboard the D/V *Chikyu*, based on the IODP protocols. We have now analyzed these onboard data, including the grain and bulk density, porosity, P-wave velocity, electrical resistivities under dry and brine-saturated conditions, permeability, magnetic susceptibility, and colorimetry (Katayama et al., 2020; Kelemen et al., 2020a, 2020b), which are summarized in Table S1. These properties were obtained from discrete core samples tha had been cut into ~2 × 2 × 2 cm cubes under laboratory temperature and pressure conditions, except for the colorimetry data that were measured continuously on whole cores with a multi-sensor core logger system. The colorimetry data correspond to the relative changes in the composition of the bulk material, and such data are widely used to correlate sections among cores or holes to analyze the characteristics of lithological changes. The measured color spectrum is normally converted to the parameters L*, a*, and b* parameters, where L* is lightness (higher value = lighter) in the range between 0 (black) and 100 (white), a* is the red–green value (higher value = redder) in the range between –60 (green) and 60 (red), and b* is the yellow–blue value (higher value = yellower) in the range between –60 (blue) and 60 (yellow). The methods of measurement and analysis for each physical property have been described by Kelemen et al. (2020c) and Katayama et al. (2020), and they are also summarized here in the Supplementary Material.

Fig. 2 shows the depth variations in the compiled physical properties for Holes BA1B and BA4A. The grain and bulk densities tend to increase with depth (grain density ranges from 2.5 to 3.0 g/cm^3), porosity tends to decrease from ~10% to <1% with increasing depth, and the P-wave velocity tends to increase from ~4 to ~6 km/s. The wet resistivity (10^1–10^4 Ωm) tends to be a few orders of magnitude lower than the dry resistivity (10^3–10^4 Ωm), and the differences are large in the dunite-dominant sequence of Hole BA1B (0–160 m). This results in a wide range of permeability from 10^{-15}–10^{-24} m^2 and clear depth variations in Hole BA1B. Magnetic susceptibility and colorimetry values are relatively high at shallow depths (0–40 m). These depth trends for each physical property are more obvious in Hole BA4A than in Hole BA1B, possibly because Hole BA1B is longer and shows clear lithological variations. The relationships among these physical properties are shown in Fig. S1 (Supplementary materials).

3.3 Independent component analysis

ICA is a powerful signal processing technique that aims to separate a multivariate signal into additive, statistically independent components (ICs). This approach is used to uncover hidden factors that contributes to the observed data, assuming that the components are statistically independent and non-Gaussian. It has been applied in various fields (e.g., signal processing) and can extract independent geological processes from a geochemical dataset (Iwamori and Albarède, 2008; Yasukawa et al., 2016).

In essence, the observed multivariate data are assumed to be linear mixtures of unknown latent variables, without any assumption about the specific processes by which this variable mix was made. ICA can be formulated mathematically as:

$$\boldsymbol{X} = \boldsymbol{S}\boldsymbol{A}, \tag{1}$$

where $\boldsymbol{X}$ is the observed data matrix whose elements $X_{i,j}$ represent the observed values for the jth variable of the ith sample, $\boldsymbol{S}$ is the independent source matrix, and $\boldsymbol{A}$ is the linear mixing matrix. The matrix $\boldsymbol{S}$ obtained through ICA represents the image of the observed data $\boldsymbol{X}$ in an r-dimensional independent component space. Each row of $\boldsymbol{S}$ corresponds to a given sample, and each column of $\boldsymbol{S}$ corresponds to the extracted independent components. These independent components serve as new variables to represent the observed data. The values of each variable in $\boldsymbol{S}$ represent coordinates in the space defined by the independent components, and these coordinates are defined as independent component scores (IC scores). The matrix $\boldsymbol{A}$ is the collection of the basis vectors (i.e., loadings) that represent the contributions of the original variables (each physical property) to the independent components obtained. A variable with a large independent component loading can be a physical property that characterizes the independent component. The positive and negative loadings correspond to the positive and negative correlations between the variables contributing to the independent component. For a given independent component, if the loadings of two variables are either positive or both negative, then they have

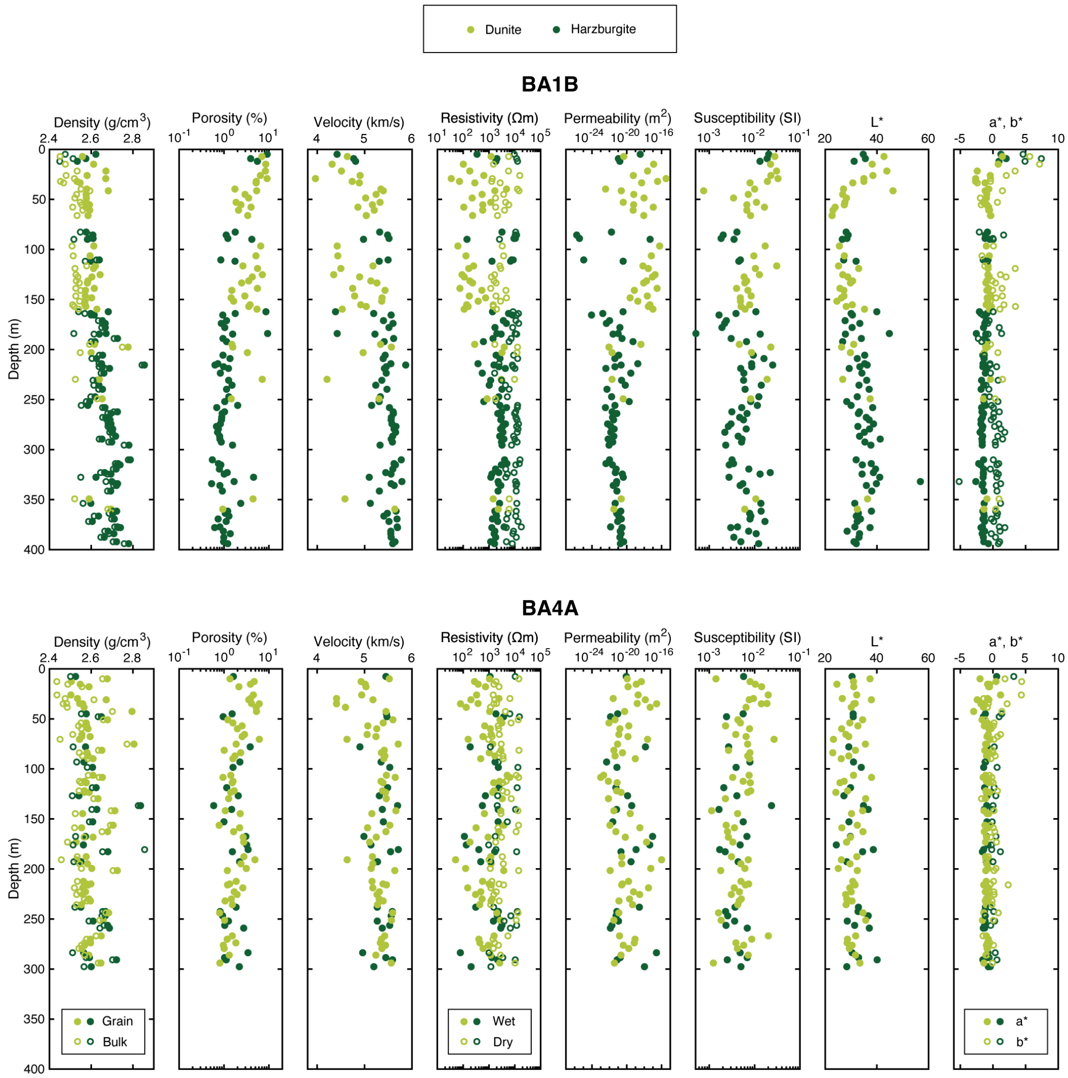

Fig. 2 Depth variations in the physical properties of discrete core samples from Holes BA1B and BA4A. The physical properties were obtained from the core descriptions and measurements made onboard the D/V *Chikyu* during the core description campaigns (Katayama et al., 2020; Kelemen et al., 2020a, 2020b). Light and dark green symbols represent dunite and harzburgite samples, respectively.

a positive correlation; if the loadings have different signs, they have a negative correlation. This information is important in deciphering the processes that underlie the data.

Successful application of the ICA algorithm and the extraction of meaningful independent components requires some data preprocessings. Following standardization, Principal Component Analysis (PCA) is employed to reduce dimensionality, transforming the dataset into uncorrelated principal components while preserving the essential characteristics of the data. By simplifying the data, PCA results in improved computational efficiency, paving the way for a more effective ICA analysis. Fig. S2 shows eigenvalues of the principal components and their contributions to the total variance in our dataset. The first four principal components account for ~85% of the variance, which is sufficient for performing ICA (Ueki and Iwamori, 2017). Therefore, we took the vectors of the first four principal components for the following ICA computation to extract four independent components.

We applied the above processes to our dataset of physical properties, which included bulk/grain density, porosity, P-wave velocity, dry/wet electrical resistivity, permeability, magnetic susceptibility, and colorimetry data, and we used these contents as variables in the observed data matrix $\boldsymbol{X}$. The histograms of the physical properties indicate multimodal, concave, or long-tailed distributions (Fig. S1). These observations reflect the inherent non-Gaussian distributions and justify the application of ICA for indentifying the factors that underlie the variations in physical properties within the Samail ophiolite. Computations of ICA were performed with the FastICA algorithm by utilizing the MATLAB fastICA package (Gävert et al., 2005: https://research.ics.aalto.fi/ica/fastica/), with some modifications. Note that the ICs cannot simply be ranked by their proportion of data variance as in PCA, because the ICs are independent. Thus, the numbering of the ICs is commutative, and there is no way to measure the relative importance of the ICs.

4 Results

Fig. 3 shows the shape of each vector obtained by ICA, from which we can infer the correlation between the physical properties. For simplicity, the loading of grain density is set as negative for all vectors. The contribution of each IC to the physical properties is highly variable. This means that at least four independent processes that affected the physical properties can be successfully extracted, which possibly reflects the processes of alteration that affected mantle peridotites in the Samail ophiolite.

The depth variations of each IC score for Holes BA1B and BA4A are shown in Fig. 4. Each IC shows a different trend with depth, which is particularly evident in Hole BA1B, as would be expected from the depth variation in physical properties (Fig. 2). IC1 tends to increase with increasing depth in Hole BA1B (Fig. 4a), whereas IC2 shows high scores in the dunite–dominant sequence in Hole BA1B (0–160 m, Fig. 4b). Although IC3 shows no clear trend with depth, some samples have markedly small values of less than −2 (Fig. 4c, g). IC4 is characterized by rapid changes at shallow depths of the holes (0–40 m, Fig. 4d, f). These results suggest that the alteration processes represented by the ICs were dominant at different depths, possibly reflecting variations in a geological factor or the environment in which the alteration occurred.

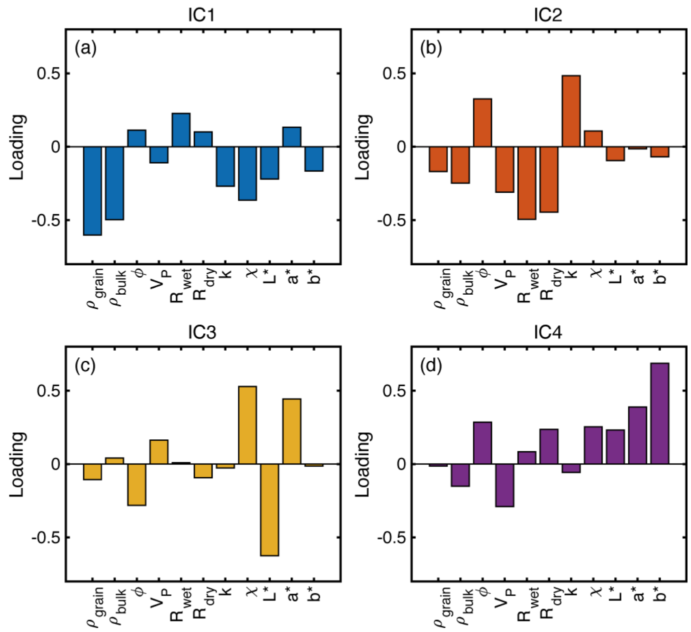

Fig. 3 Relative loadings of each physical property for IC1 to IC4. Abbreviations are; ρ_{grain}= grain density, ρ_{bulk}= bulk density, ϕ= porosity, V_{P}= P-wave velocity, R_{dry}= dry resistivity, R_{wet}= wet resistivity, k= permeability, χ= magnetic susceptibility.

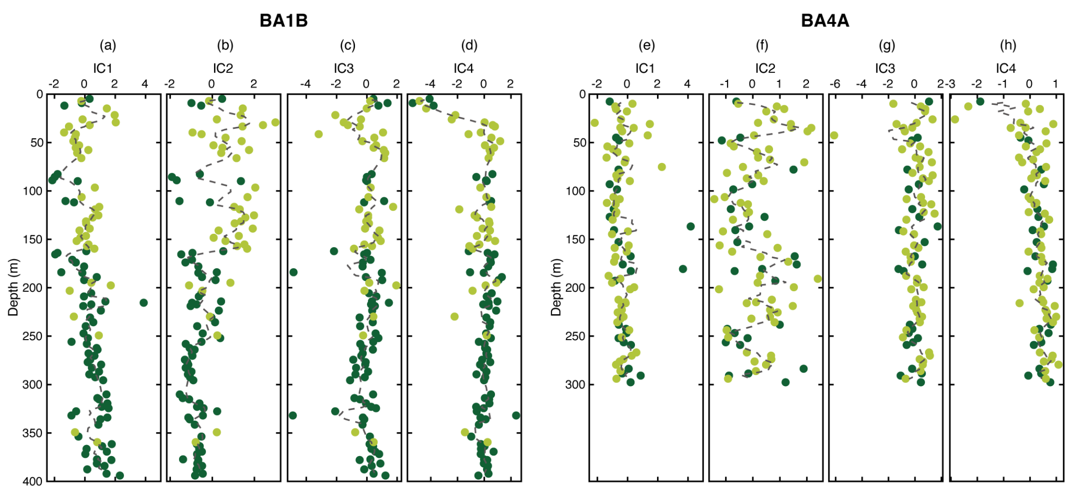

Fig. 4 Depth variations in each independent component for Holes BA1B (a–d) and BA4A (e–h). Light and dark green symbols represent dunite and harzburgite samples, respectively. The dashed lines are five-point moving averages.

5 Interpretation of the independent components

Our interpretation of the ICA results was based on the IC loadings (Fig. 3) and IC scores (Fig. 4). The IC loadings indicate the proportional contributions of each physical property to each IC, whereas IC scores denote the coordinate values of the sample data within the IC space. We used Eq. 1 and the loadings and scores to quantify the contribution of each IC to the variations in each physical property. Here, we obtained the difference between the maximum and minimum back-calculated values of physical properties as ΔX (or $\Delta \log X$) to quantitatively assess the contributions of ICs to each physical property (Fig. 5). Through linear transformation, each IC can also be represented as a vector in scatter plots (Fig. 6 and Supplementary Materials Fig. S2). Fig. 7 shows scatter plots of each IC score as a function of the degree of hydration (d), which is estimated empirically from grain density (ρ_{grain}) as $d = (3.3 - \rho_{\mathrm{grain}})/0.785$ (Miller and Christensen, 1997): Our IC interpretations also involved comparing these results with the petrological and geochemical characteristics of the core samples, as reported in previous studies (Ellison et al., 2021; Kelemen et al., 2021).

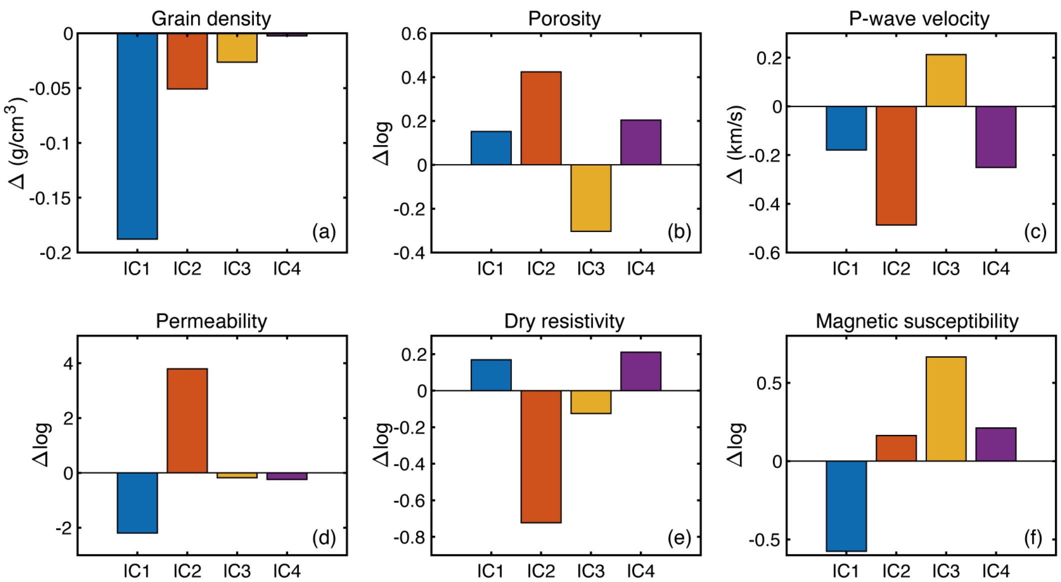

Fig. 5 Difference between the maximum and minimum back-calculated values of physical properties (ΔX or $\Delta \log X$): (a) grain density, (b) porosity, (c) P-wave velocity, (d) permeability, (e) dry resistivity, and (f) magnetic susceptibility. The sign is aligned with the loading.

5.1 IC1: Early stage of serpentinization

IC1 is characterized by a significant decrease in grain/bulk density compared with the other ICs (Fig. 3a), with the variation in grain density of approximately –0.2 g/cm^3 (Fig. 5a). This means that the replacement of olivine by serpentine predominates during this process, increasing the degree of hydration. With the progress of hydration, porosity increases by ~1.5% ($\Delta \log \sim 0.2$) and the P-wave velocity decreases by ~0.2 km/s

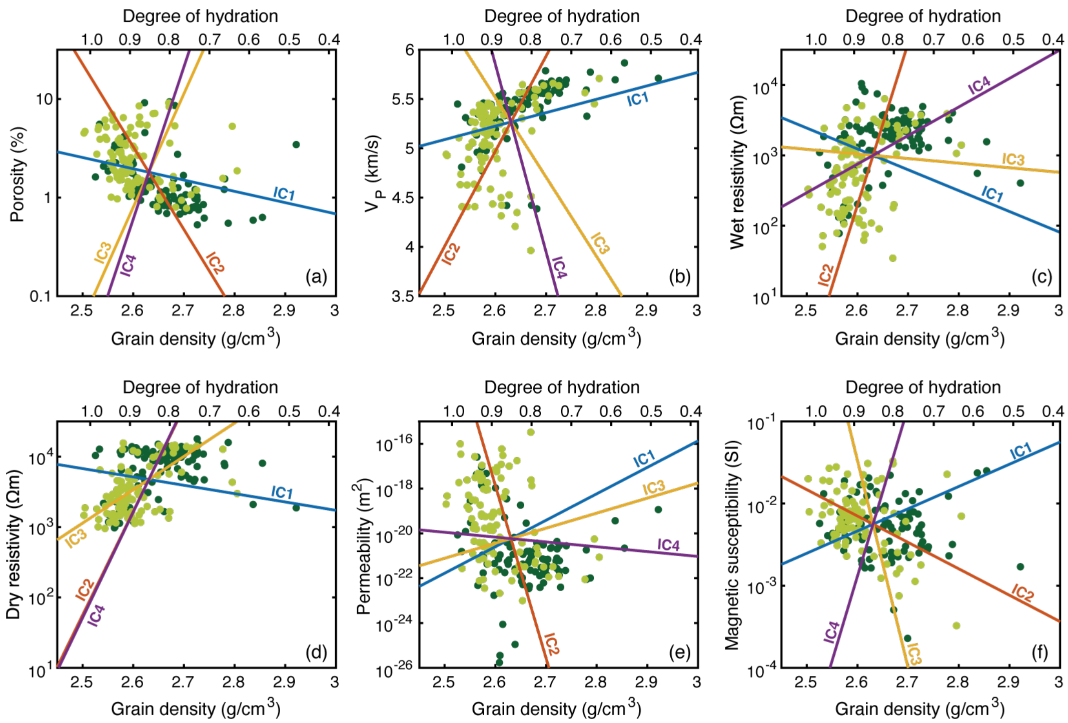

Fig. 6 Scatter plots of (a) porosity, (b) P-wave velocity, (c, d) wet and dry resistivity, (e) permeability, and (f) magnetic susceptibility as a function of grain density, plotted with independent component vectors. The degree of hydration, calculated from grain density, is also shown on the upper horizontal axis. Light and dark green symbols represent dunite and harzburgite samples, respectively.

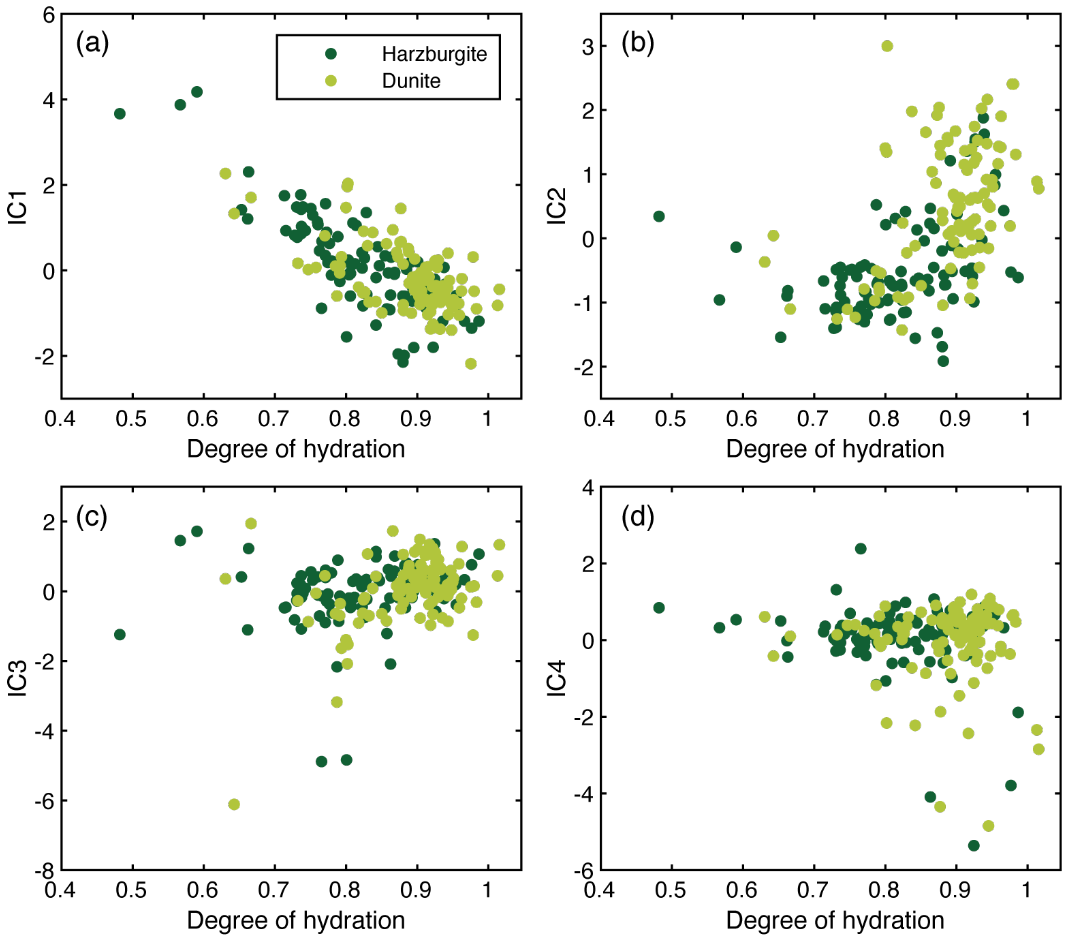

Fig. 7 Independent components as functions of the degree of hydration, which is inferred from grain density. Light and dark green symbols represent dunite and harzburgite samples, respectively.

(Fig. 5a–c). The negative correlation between porosity and P-wave velocity suggests that spheroidal (penny-shaped) cracks, which reduce the elastic moduli of rocks (Guéguen and Kachanov, 2011), are formed during this process while the degree of hydration increases. Although crack development typically leads to an increase in permeability due to the formation of a crack network with increasing in crack density (Guéguen and Palciauskas, 1994), the IC1 characteristics show that porosity can increase at the same time as permeability decreases during alteration (Figs. 3, 5). This suggests that the IC1 process causes clogging of the connected cracks or the formation of isolated cracks. The volume dilation that accompanies serpentinization results in the clogging of cracks in the porous rock (Macdonald and Fyfe, 1985; Ulven et al., 2014; Uno et al., 2022), and several mechanisms can lead to the formation of isolated cracks. For example, connected and isolated cracks could both be formed as a result of the stress generated by volume dilation (i.e., reaction-driven cracking, Okamoto and Shimizu, 2015; Yoshida et al., 2020) during the early stage of serpentinization (d>0.2, Rouméjon and Cannat, 2014). Moreover, alteration products (serpentine) would contain partially connected intrinsic submicron-scale pores (Plümper et al., 2017; Tutolo et al., 2016). Therefore, the progress of serpentinization can lead simultaneously to an increase in porosity and a decrease in permeability. Moreover, the IC1 score is high at d=~0.6 and decreases with d increases to 1.0 (Fig. 7a). Given these results, our interpretation is that IC1 represents the alteration of olivine to serpentine during the early stage of serpentinization that proceeds under a rock-dominated system (Bach et al., 2006).

5.2 IC2: Later-stage of serpentinization

IC2 reflects a process that produced drastic changes in various physical properties. Despite a small decrease in grain/bulk density (increases in d) relative to IC1, porosity increased by ~2.5% and P-wave velocity decreased by ~0.4 km/s (Fig. 5a–c and Fig. 6a, b). These values indicate that the development of cracks during the IC2 process was more extensive than that during IC1. Wet resistivity shows a clear negative correlation with porosity (Fig. 3b), and this results in an increase in permeability by up to four orders of magnitude (Fig. 5d). Strong correlations between porosity and electrical resistivity or permeability (i.e., transport properties) also suggest that crack development during this process involved the formation of a crack network, since transport properties are highly sensitive to crack connectivity (Guéguen and Palciauskas, 1994). The crack interconnections (i.e., percolation) tend to increase abruptly when the crack density exceeds a certain threshold, resulting in significant changes in the transport properties (Guéguen and Dienes, 1989). Such percolative behavior may lead to further fluid infiltration and serpentinization in a relatively open system (i.e., with a high water–rock ratio, Bach et al., 2006; Jamtveit et al., 2008; Kelemen and Hirth, 2012; Okamoto and Shimizu, 2015) This is consistent with that the IC2 scores starting to increase steeply at $d =\sim 0.9$ (Fig. 7b). Therefore, IC2 corresponds to the alteration of olivine to serpentine accompanied by extensive crack development during the later stage of primary serpentinization.

IC2 scores are generally larger for dunite samples than for harzburgite samples in Hole BA1B (Fig. 4b), which suggests that the later-stage serpentinization in an open-system tends to be more dominant for dunite than for harzburgite. Fig. 8 shows representative microstructures of samples with relatively high and low IC2 scores. The dunite sample (BA1B-40Z-2) with an IC2 score of 2.04 exhibits a mesh texture, which is typical of low-temperature serpentinization, and only a few relics of olivine and orthopyroxene remain (Fig. 8a). Olivine relics can be seen in the harzburgite sample (BA1B-134Z-4) that has a relatively low IC2 score (–1.38). These observations suggest that samples with high IC2 scores are characterized by exhaustive serpentinization due to the progressive fracturing–reaction processe and positive feedbacks. Alternatively, the degree of later-stage serpentinization represented by IC2 could depend on the protolith, since harzburgite contains relatively small amounts of primary olivine compared with dunite.

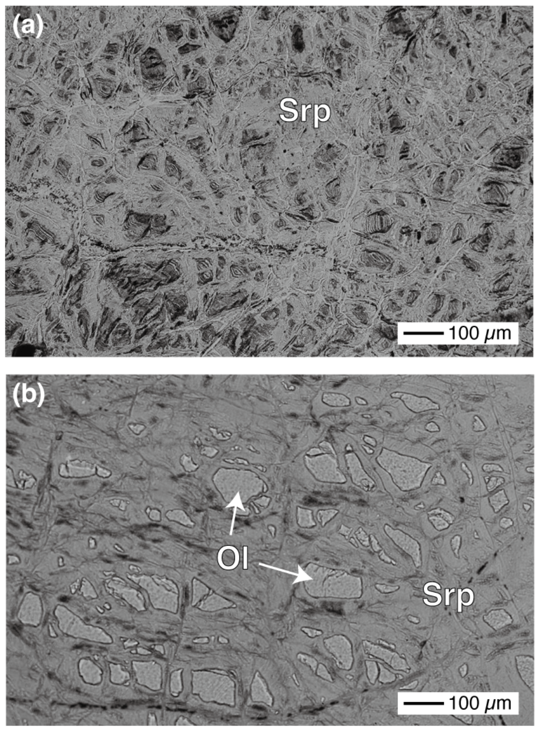

Fig. 8 Photomicrographs showing the microstructures of representative samples with relatively high and low IC2 scores, modified after Katayama et al. (2021). (a) BA1B-40Z-2 (dunite). (b) BA1B-134Z-4 (harzburgite). Mineral abbreviations: Srp = serpentine, Ol = olivine.

5.3 IC3: Magnetite formation related to local silica activity

IC3 represents a process that caused a significant increase in magnetic susceptibility with decreasing grain density (Fig. 3c). As magnetic susceptibility is mainly a reflection of the amount of magnetite (Oufi et al., 2002), IC3 could be associated with a marked increase in magnetite content. The IC3 scores increase slightly with the degree of hydration, indicating that magnetite forms slowly during serpentinization (Fig. 7c). The IC3 scores show no clear trend with depth, and some samples locally show extremely low values (Fig. 4c, g). This suggests that the formation of magnetite during the IC3 process could be influenced by differences in the local chemical conditions that might have controled the nucleation of magnetite (e.g., fluid composition and redox conditions). IC3 is also characterized by a strong negative correlation between magnetic susceptibility and L*, which means that whitish rocks have lower magnetism. The whitish areas of the core samples are pyroxene-rich (Fig. 9) and have been partially altered to talc with an absence of magnetite (Fig. 9f) due to high silica activity related to the presence of pyroxene (Katayama et al., 2010). Large magnetite grains often exist along the rims of spinel grains in the cores from Holes BA1B and BA4A, and these possibly resulted from the alteration of Fe–Cr spinel (Hong et al., 2022). Some of the samples that contain magnetite on spinel rims have high IC3 scores. The negative loading in porosity may indicate that the formation of magnetite during the IC3 process was not necessarily accompanied by crack development, whereas talc formation involves a marked dilation of the rock, which may cause cracking. Thus, IC3 reflects serpentinization with the formation of magnetite, and its variations with depth may reflect the spatial distribution of silica activity.

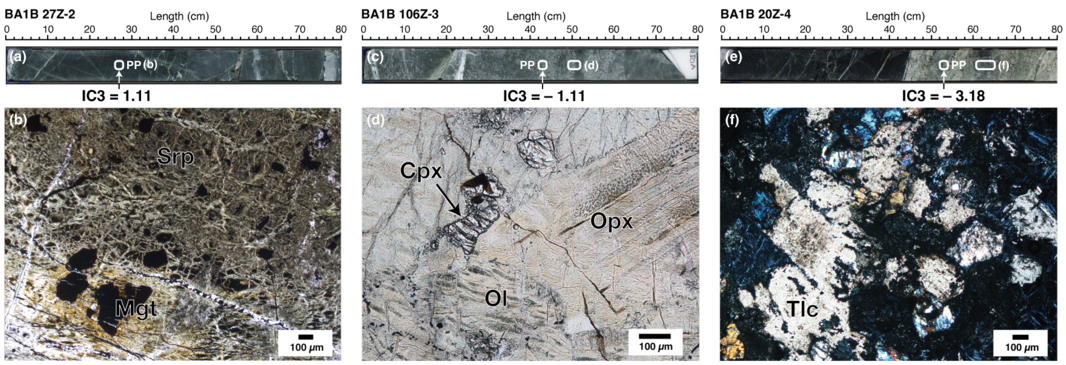

Fig. 9 Representative core sections from which discrete samples with characteristic IC3 scores were collected: (a) BA1B 57Z-2, (c) BA1B 106Z-3, and (e) BA1B 20Z-4. Location of each thin section (b, d, f) is indicated as white squares, and the white squares with "PP" indicate the location of each discrete sample. Mineral abbreviations: Srp = serpentine, Mgt = magnetite, Ol = olivine, Opx = orthopyroxene, Cpx = clinopyroxene, Tlc = talc.

5.4 IC4: Subsurface weathering/carbonation

IC4 involves an increase in porosity and a decrease in P-wave velocity, with no marked change in grain density (Fig. 3d). Thus, like IC1 and IC2, the IC4 process is related to crack development, although the degree of hydration (d) remains unchanged (Fig. 7d). IC4 is also characterized by clear positive loadings in colorimetry (Fig. 3d), particularly for b* (yellowness), whereas the other ICs were not related to b* (Fig. 3a–c). Since the colorimetry data signal relative changes in the composition of the bulk material, these results suggest that the IC4 process was related to processes of alteration that differed from the typical serpentinization represented by the other ICs. The IC4 scores change sharply with depth, with the shallower parts of the two holes characterized by low scores (Fig. 4d, h). This suggests that the IC4 process was associated with a near-surface process in the Samail ophiolite that was independent of the primary serpentinization.

The surface of the mantle section of the Samail ophiolite is subjected to ongoing weathering and carbonation at temperatures of $<50^{o}$C (Kelemen and Matter, 2008). Carbonation of an ultramafic body proceeds by the reaction of olivine and serpentine with CO_2 at low temperature and the formation of carbonate minerals such as calcite ($CaCO_3$) and magnesite ($MgCO_3$). The quantities of CO_2 and calcite veins in Hole BA1B, that were reported by the shipboard descriptions (Kelemen et al., 2020a), tend to be higher at depths of <50 m (Fig. 10a, b). This is consistent with the depth variation in the IC4 score with depth (Fig. 4d) and microstructural observations of a sample showing low IC4 score (Fig. 10c, d). Similar trends can be seen for Hole BA4A. The carbonation of ultramafic rocks results in the development of cracks due to reaction-induced dilation as well as serpentinization (Kelemen and Hirth, 2012), and this is consistent with the increase in porosity and decrease in velocity during the IC4 process (Fig. 3d and Fig. 6a, b). Weathering occurs in an oxidizing environment and is often accompanied by a change in the color of a rock to reddish or yellowish, which can be attributed to the formation of Fe oxides (Yokoyama and Nakashima, 2005). This is also consistent with the clear correlation between a* (redness) or b* (yellowness) and IC4, which can be confirmed by direct observations of the core sections (Fig. 10c, d). Consequently, these features suggest that IC4 reflects the carbonation of mantle peridotite during ongoing weathering under atmospheric conditions.

IC4 is also related to an increase in magnetic susceptibility (Fig. 3d), which suggests that magnetite is formed alongside carbonate during this process. Formation of Mg-carbonates by the reaction of CO_2 with peridotite is often accompanied by the release of dissolved SiO_2 (Streit et al., 2012), and this may be the source of SiO_2 for the silicification of ferroan brucite, which results in the additional formation of magnetite. Such carbotation-related magnetites are found along with a calcite vein in our sample (Fig. 10d).

6 Discussion

6.1 Multiple stages of alteration extracted via ICA

We applied ICA to a dataset of the multivariate physical properties of mantle peridotites in the Samail ophiolite, as described and measured onboard the D/V *Chikyu*. This allowed us to extract four independent components that represent different processes of alteration. IC1 corresponds to early stage of serpentinization, where olivine is replaced by serpentine. This process involved reaction-induced cracking, although its impact on fluid transportation was limited. IC2 corresponds to later-stage of serpentinization, which was accompanied by extensive cracking and marked changes in elastic and transport properties. IC3 represents the formation of magnetite, which was associated with reactions that differed from those of the primary serpentinization (IC1 and IC2). IC4 captures the ongoing carbonation near the present-day surface of the ophiolite, which involves a reduction in elastic wave velocity due to reaction-induced cracking and the formation of additional magnetite during associated silicification.

The Samail ophiolite was formed in a supra-subduction zone, in which obduction started during or immediately after the formation of crust at a relatively fast-spreading ridge (Rioux et al., 2012). The mantle peridotites in the Samail ophiolite have therefore undergone multiple stages of deformation and alteration. Trace-element and oxygen isotope geochemistry of serpentinite from the BA site suggest that serpentinization took place below a thick magmatic crust in an off-axis setting (Aupart et al., 2021). Thus, the constrained hydration processes (IC1–3) would represent hydrothermal alteration in a mid-oceanic ridge setting. We found that IC2 and IC3 feature an increase in magnetic susceptibility as

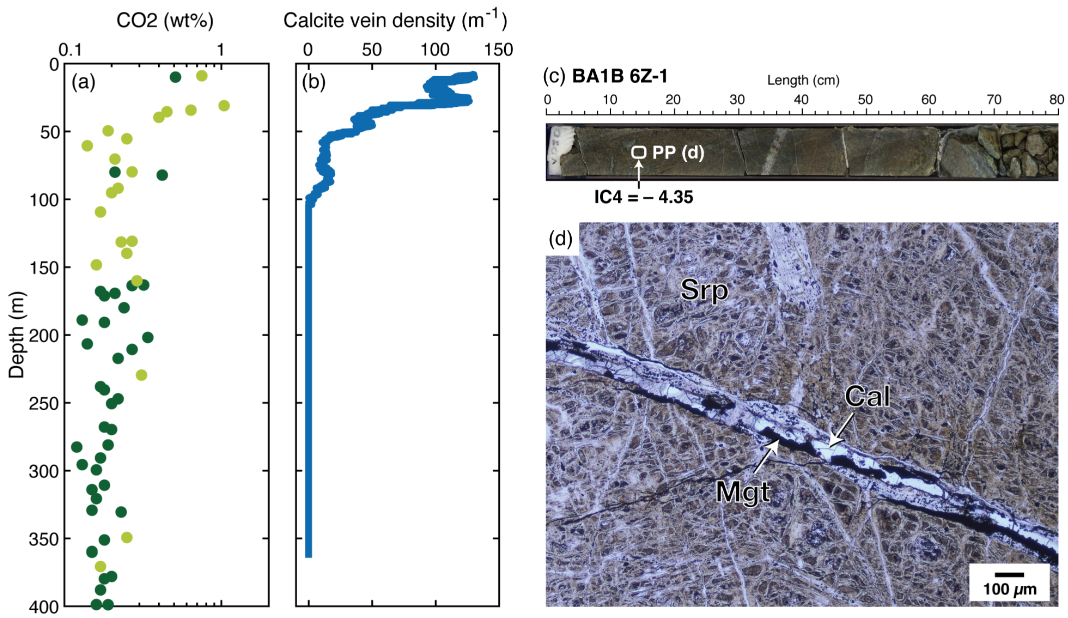

Fig. 10 Variations with depth in (a) CO_2 content and (b) calcite vein density in Hole BA1B and a representative core section (c) from which a discrete sample with low IC4 score was collected (BA1B 6Z-1). Location of the discrete sample is indicated as a white square. Thin section image (d) shows a calcite vein with magnetite and oxidized serpentine matrix. The data and image (a–c) are modified after Kelemen et al. (2020a). Mineral abbreviations: Srp = serpentine, Mgt = magnetite, Cal = calcite.

hydration progressed, suggesting that hydrogen is produced in a mid-oceanic ridge setting in association with the formation of magnetite. Since IC4 also involves magnetite formation, the hydrogen production may be still active after the ophiolite obduction, as Ellison et al. (2021) identified the production of hydrogen and hydrocarbons in the Samail ophiolite as a result of modern water–rock interactions. Our study suggests that altered mantle peridotites in the Samail ophiolite may record multiple episodes of hydrogen production occurring in both submarine and subaerial environments.

The alteration of mantle rocks has been revealed by geophysical surveys in various tectonic settings, including oceanic core complexes near slow-spreading ridges and transform faults (Muller et al., 1997; Okino et al., 2004), and in outer-rise regions along subduction zones (Fujie et al., 2013; Grevemeyer et al., 2007; Ranero et al., 2003). These mantle peridotites probably undergo deformation and alteration under temperature and pressure conditions that differ from those recorded by the Samail ophiolite. Indeed, some peridotite samples that were recovered by dredging or drilling on the seafloor exhibit trends in physical properties that differ from those analyzed in the present study (Fujii et al., 2016; Kelemen et al., 2004). Our results show that ICA is an effective tool for extracting and understanding complex physicochemical processes of mantle alteration, using a dataset of physical properties for the Samail ophiolite. Therefore, the application of ICA to similar datasets for mantle rocks from a variety of tectonic settings may reveal geological processes that are unique to each tectonic environment.

6.2 Geophysical implications

6.2.1 Effects of reaction-induced cracking on seismic velocity

Serpentinization has been associated with low seismic velocity anomalies in areas where seawater can penetrate the mantle through fracture zones (Minshull et al., 1991; Minshull and White, 1996; Ranero et al., 2003). The effect of serpentinization on seismic velocity is generally attributed to the conversion of olivine to serpentine (Christensen, 2004), which is consistent with the significant decrease in grain density (increase in the degree of hydration) that characterizes the IC1 process (Fig. 5a). However, our results show that the increase in porosity is larger during the IC2 process than during the IC1 process (Fig. 5b), and the effect of reaction-induced cracking on seismic velocity is large during the IC2 process (Fig. 5c). These observations may indicate that the effect of the alteration of olivine to serpentine on P-wave velocities is predominant during earlier serpentinization reactions (d<0.6), when crack formation is limited, and that the effect of cracks becomes crucial when interpreting the geophysical anomalies observed in regions where the degree of hydration is high (Hatakeyama and Katayama, 2020).

We also identified relatively large increases in porosity and decreases in P-wave velocity during the IC4 process, which are almost comparable to those in IC1 (Fig. 5b, c). The generation of such carbonation and porosity generation had already been observed in natural samples collected from the seafloor (e.g., Bach et al., 2011; Jöns et al., 2017). Our results imply that the presence of carbonated mantle rocks on the seafloor may also be indicated by a low-seismic velocity anomaly, and this could be important in terms of the global carbon budget from geophysical observations (Katayama et al., 2023).

Although processes other than IC3 involve crack development, only IC2 exhibits a significant increase in permeability (Fig. 5d). This may indicate differences in the water–rock ratio for each reaction process. The water–rock ratio during alteration reactions can have a large impact on the compositions of the alteration products. Katayama et al. (2023) modeled the effect on seismic velocity of variations in reaction products during the alteration of mantle rocks, based on thermodynamic modeling, and they discussed the potential role of water–rock ratios in assessing global carbon budgets from interpretations of seismic velocity structures. Our results may provide new constraints on such thermodynamic modeling and the interpretation of geophysical data.

6.2.2 Effect of magnetite formation on electrical and magnetic properties

We found that both dry and wet resistivity decrease with increasing porosity during the IC2 process (Fig. 5d). The decrease in wet resistivity reflects the percolation of cracks, whereas the decrease in dry resistivity suggests the formation and connection of conductive minerals (Guéguen and Palciauskas, 1994). Magnetite is one of the typical secondary minerals that are formed during the hydration of peridotite, and magnetite formation is associated with the breakdown of ferroan brucite or serpentine under open-system conditions (Bach et al., 2006; Frost and Beard, 2007). The occurrence of magnetite is often associated with a low dry resistivity in serpentinized peridotite (Katayama et al., 2020; Kawano et al., 2012). Therefore, it is possible that percolation through reaction-induced cracks and the formation of magnetite network took place during in the later stage of primary serpentinization.

We also identified an increase in magnetic susceptibility that can be related to the formation of magnetite during the IC2, IC3 and IC4 processes (Fig. 5f). As magnetic susceptibility reflects the formation of magnetite and serves as an indicator of the amount of hydrogen produced during magnetite formation, our observations may indicate differences in the amount of hydrogen produced during each reaction process. However, these changes do not coincide with the changes in dry resistivity (Fig. 5), despite both depending strongly on the formation of magnetite. This result can be attributed to the different sensitivities of magnetic and electrical properties to the distribution of magnetite in the rock. Magnetic susceptibility depends mainly on the volume fraction of magnetic minerals (Oufi et al., 2002), while electrical resistivity depends mainly on the degree of interconnection of conductive phases (Guéguen and Palciauskas, 1994). In the altered peridotites collected during the Oman Drilling Project, three types of magnetite occurrence were observed (Hong et al., 2022): (i) elongated veins in areas of mesh texture, (ii) the overgrowth rims on spinel, and (iii) as aggregates of small grains in the serpentine matrix. Magnetites with the second and third types of occurrences tend to be sparsely distributed in the serpentinized peridotite. Therefore, their occurrence would not form a conductive path on the scale of the sample, thus resulting in an increase of magnetic susceptibility without a marked decrease in resistivity. Our results suggest that the distribution of magnetite in the rock varies with the reaction conditions, and different distributions result in different electrical and magnetic properties. This implies that the occurrences of magnetic and electrical anomalies do not necessarily coincide during the process of mantle alteration.

7 Conculusions

To understand the structure of the data in a dataset of physical properties and to investigate the processes of alteration of mantle peridotite, we subjected the physical properties of altered peridotite collected from the Samail ophiolite during the Oman Drilling Project to independent component analysis (ICA). Four independent components accounted for 85% of the variations in physical properties. Combining these results with the petrological and geochemical data reported in previous studies, we concluded that the four independent components represent early-stage of serpentinization, later-stage of serpentinization, magnetite formation, and near-surface carbonation. The ICA results indicate that the effect of alteration on the physical properties of the mantle peridotite in the Samail ophiolite varied from process to process. Our results show that multivariate analysis can be applied to high-dimensional datasets of rock physical properties, and such analyses will provide new insights into the processes of mantle alteration processes from a geophysical point of view.

Data availability

All the physical property data and our analytical results are summarized in Supplementary Table S1. The original data are archived on the ICDP website (https://www.icdp-online.org/projects/by-continent/asia/oodp-oman). The electrical resistivity data we used in this study were those re-measured by Katayama et al. (2020) and archived at https://doi.org/10.1594/PANGAEA.913501.

Acknowledgements

We thank the science party of the Oman Drilling Project and all those who conducted the drilling and made the measurements of physical properties onboard the D/V *Chikyu*. We are also grateful to Prof. H. Hino for his useful comments on the data analyses, Prof. I. Katayama for providing photomicrographs core samples, Dr. N. Abe for providing core samples for microstructural observations, and Dr. T. Togo for making thin sections. This study was supported by the Japan Society for the Promotion of Science KAKENHI (Grant 23KJ2219) and JST CREST (JPMJCR1761).

References

Aupart, C., Morales, L., Godard, M., Jamtveit, B., 2021. Seismic faults triggered early stage serpentinization of peridotites from the samail ophiolite, oman. Earth and planetary science letters 574, 117137. https://doi.org/10.1016/j.epsl.2021.117137

Bach, W., Paulick, H., Garrido, C.J., Ildefonse, B., Meurer, W.P., Humphris, S.E., 2006. Unraveling the sequence of serpentinization reactions: Petrography, mineral chemistry, and petrophysics of serpentinites from MAR 15°N (ODP leg 209, site 1274). Geophysical research letters 33. https://doi.org/10.1029/2006gl025681

Bach, W., Rosner, M., Jöns, N., Rausch, S., Robinson, L.F., Paulick, H., Erzinger, J., 2011. Carbonate veins trace seawater circulation during exhumation and uplift of mantle rock: Results from ODP leg 209. Earth and planetary science letters 311, 242–252.

https://doi.org/10.1016/j.epsl.2011.09.021
Boudier, F., Baronnet, A., Mainprice, D., 2010. Serpentine mineral replacements of natural olivine and their seismic implications: Oceanic lizardite versus subduction-related antigorite. Journal of Petrology 51, 495–512. https://doi.org/10.1093/petrology/egp049
Christensen, N.I., 2004. Serpentinites, peridotites, and seismology. International geology review 46, 795–816. https://doi.org/10.2747/0020-6814.46.9.795
Ellison, E.T., Templeton, A.S., Zeigler, S.D., Mayhew, L.E., Kelemen, P.B., Matter, J.M., The Oman Drilling Project Science Party, 2021. Low-temperature hydrogen formation during aqueous alteration of serpentinized peridotite in the samail ophiolite. Journal of Geophysical Research, [Solid Earth] 126. https://doi.org/10.1029/2021jb021981
Escartín, J., Hirth, G., Evans, B., 1997. Effects of serpentinization on the lithospheric strength and the style of normal faulting at slow-spreading ridges. Earth and planetary science letters 151, 181–189. https://doi.org/10.1016/s0012-821x(97)81847-x
Ferrand, T.P., Hilairet, N., Incel, S., Deldicque, D., Labrousse, L., Gasc, J., Renner, J., Wang, Y., Green, H.W., Ii, Schubnel, A., 2017. Dehydration-driven stress transfer triggers intermediate-depth earthquakes. Nature communications 8, 15247. https://doi.org/10.1038/ncomms15247
Frost, B.R., Beard, J.S., 2007. On silica activity and serpentinization. Journal of Petrology 48, 1351–1368. https://doi.org/10.1093/petrology/egm021
Fujie, G., Kodaira, S., Yamashita, M., Sato, T., Takahashi, T., Takahashi, N., 2013. Systematic changes in the incoming plate structure at the kuril trench. Geophysical research letters 40, 88–93.
Fujii, M., Okino, K., Sato, H., Nakamura, K., Sato, T., Yamazaki, T., 2016. Variation in magnetic properties of serpentinized peridotites exposed on the yokoniwa rise, central indian ridge: Insights into the role of magnetite in serpentinization. Geochemistry, Geophysics, Geosystems 17, 5024–5035. https://doi.org/10.1002/2016GC006511
Gävert, H., Hurri, J., Särelä, J., Hyvärinen, A., 2005. The FastICA package for MATLAB.
Grevemeyer, I., Ranero, C.R., Flueh, E.R., Kläschen, D., Bialas, J., 2007. Passive and active seismological study of bending-related faulting and mantle serpentinization at the middle america trench. Earth and planetary science letters 258, 528–542. https://doi.org/10.1016/j.epsl.2007.04.013
Guéguen, Y., Dienes, J., 1989. Transport properties of rocks from statistics and percolation. Mathematical geology 21, 1–13. https://doi.org/10.1007/BF00897237
Guéguen, Y., Kachanov, M., 2011. Effective elastic properties of cracked rocks — an overview, in: Leroy, Y.M., Lehner, F.K. (Eds.), Mechanics of Crustal Rocks. Springer Vienna, Vienna, pp. 73–125. https://doi.org/10.1007/978-3-7091-0939-7/_3
Guéguen, Y., Palciauskas, V., 1994. Introduction to the physics of rocks. Princeton University Press.
Hatakeyama, K., Katayama, I., 2020. Pore fluid effects on elastic wave velocities of serpentinite and implications for estimates of serpentinization in oceanic lithosphere. Tectonophysics 775, 228309. https://doi.org/10.1016/j.tecto.2019.228309
Hatakeyama, K., Katayama, I., Hirauchi, K.-I., Michibayashi, K., 2017. Mantle hydration along outer-rise faults inferred from serpentinite permeability. Scientific reports 7. https://doi.org/10.1038/s41598-017-14309-9
Hong, G., Till, J.L., Greve, A., Lee, S.-M., the Oman Drilling Project Phase 2 Science Party, 2022. New rock magnetic analysis of ultramafic cores from the oman drilling

project and its implications for alteration of lower crust and upper mantle. Journal of Geophysical Research, [Solid Earth] 127. https://doi.org/10.1029/2022jb024379

Hyvärinen, A., Karhunen, J., Oja, E., 2001. Independent component analysis. John Wiley & Sons.

Iwamori, H., Albarède, F., 2008. Decoupled isotopic record of ridge and subduction zone processes in oceanic basalts by independent component analysis. Geochemistry, Geophysics, Geosystems 9. https://doi.org/10.1029/2007GC001753

Iwamori, H., Yoshida, K., Nakamura, H., Kuwatani, T., Hamada, M., Haraguchi, S., Ueki, K., 2017. Classification of geochemical data based on multivariate statistical analyses: Complementary roles of cluster, principal component, and independent component analyses. Geochemistry, Geophysics, Geosystems 18, 994–1012. https://doi.org/10.1002/2016gc006663

Jamtveit, B., Malthesorenssen, A., Kostenko, O., 2008. Reaction enhanced permeability during retrogressive metamorphism. Earth and planetary science letters 267, 620–627. https://doi.org/10.1016/j.epsl.2007.12.016

Jöns, N., Kahl, W.-A., Bach, W., 2017. Reaction-induced porosity and onset of low-temperature carbonation in abyssal peridotites: Insights from 3D high-resolution microtomography. Lithos 268-271, 274–284. https://doi.org/10.1016/j.lithos.2016.11.014

Katayama, I., Abe, N., Hatakeyama, K., Akamatsu, Y., Okazaki, K., Ulven, O.I., Hong, G., Zhu, W., Cordonnier, B., Michibayashi, K., Godard, M., Kelemen, P., the Oman Drilling Project Phase 2 Science Party, 2020. Permeability profiles across the crust-mantle sections in the oman drilling project inferred from dry and wet resistivity data. Journal of Geophysical Research, [Solid Earth] 125. https://doi.org/10.1029/2019jb018698

Katayama, I., Abe, N., Okazaki, K., Hatakeyama, K., Akamatsu, Y., Michibayashi, K., Godard, M., Kelemen, P.B., the Oman Drilling Project Phase 2 Science Party, 2021. Crack geometry of serpentinized peridotites inferred from onboard ultrasonic data from the oman drilling project. Tectonophysics 814, 228978. https://doi.org/10.1016/j.tecto.2021.228978

Katayama, I., Kurosaki, I., Hirauchi, K.-I., 2010. Low silica activity for hydrogen generation during serpentinization: An example of natural serpentinites in the mineoka ophiolite complex, central japan. Earth and planetary science letters 298, 199–204. https://doi.org/10.1016/j.epsl.2010.07.045

Katayama, I., Okazaki, K., Okamoto, A., 2023. Role of mantle carbonation in trench outer-rise region in the global carbon cycle. Island Arc 32. https://doi.org/10.1111/iar.12499

Kawano, S., Yoshino, T., Katayama, I., 2012. Electrical conductivity of magnetite-bearing serpentinite during shear deformation. Geophysical research letters 39. https://doi.org/10.1029/2012gl053652

Kelemen, P.B., Hirth, G., 2012. Reaction-driven cracking during retrograde metamorphism: Olivine hydration and carbonation. Earth and planetary science letters 345-348, 81–89. https://doi.org/10.1016/j.epsl.2012.06.018

Kelemen, P.B., Kikawa, E., Miller, D.J., Abe, N., Bach, W., Carlson, R.L., Casey, J.F., Chambers, L.M., Cheadle, M., Cipriani, A., Others, 2004. Site 1274, in: Proceedings of the Ocean Drilling Program, 209 Initial Reports. Ocean Drilling Program. https://doi.org/10.2973/odp.proc.ir.209.109.2004

Kelemen, P.B., Leong, J.A., Carlos de Obeso, J., Matter, J.M., Ellison, E.T., Templeton, A., Nothaft, D.B., Eslami, A., Evans, K., Godard, M., Malvoisin, B., Coggon, J.A., Warsi, N.H., Pézard, P., Choe, S., Teagle, D.A.H., Michibayashi, K., Takazawa, E., Al Sulaimani, Z., The Oman Drilling Project Science Team, 2021. Initial results from the oman drilling project multi-borehole observatory: Petrogenesis and ongoing alteration of mantle peridotite in the weathering horizon. Journal of Geophysical Research, [Solid Earth] 126. https://doi.org/10.1029/2021jb022729

Kelemen, P.B., Matter, J., 2008. In situ carbonation of peridotite for CO_2 storage. Proceedings of the National Academy of Sciences 105, 17295–17300. https://doi.org/10.1073/pnas.0805794105

Kelemen, P.B., Matter, J.M., Teagle, D.A.H., Coggon, J.A., the Oman Drilling Project Science Team, 2020c. Proceedings of the oman drilling project. International Ocean Discovery Program College Station, TX.

Kelemen, P.B., Matter, J.M., Teagle, D.A.H., Coggon, J.A., the Oman Drilling Project Science Team, 2020b. Site BA4, in: Kelemen, P.B., Matter, J.M., Teagle, D.A.H., Coggon, J.A., others (Eds.), Proceedings of of the Oman Drilling Project. International Ocean Discovery Program, College Station, TX. https://doi.org/10.14379/OmanDP.proc.2020

Kelemen, P.B., Matter, J.M., Teagle, D.A.H., Coggon, J.A., the Oman Drilling Project Science Team, 2020a. Site BA1, in: Kelemen, P.B., Matter, J.M., Teagle, D.A.H., Coggon, J.A., others (Eds.), Proceedings of of the Oman Drilling Project. International Ocean Discovery Program, College Station, TX. https://doi.org/10.14379/OmanDP.proc.2020

Kelemen, P.B., Shimizu, N., Salters, V.J.M., 1995. Extraction of mid-ocean-ridge basalt from the upwelling mantle by focused flow of melt in dunite channels. Nature 375, 747–753. https://doi.org/10.1038/375747a0

Kuwatani, T., Nakamura, K., Watanabe, T., Ogawa, Y., Komai, T., 2014. Evaluation of geochemical characteristics of tsunami deposits by the 2011 off the pacific cost of tohoku earthquake using dimensionality reduction with a principal component analysis. (in Japanese with English Abstract), Journal of Geography (Chigaku Zasshi) 123, 923–935. https://doi.org/10.5026/jgeography.123.923

Macdonald, A.H., Fyfe, W.S., 1985. Rate of serpentinization in seafloor environments. Tectonophysics 116, 123–135. https://doi.org/10.1016/0040-1951(85)90225-2

Miller, D.J., Christensen, N.I., 1997. Seismic velocities of lower crustal and upper mantle rocks from the slow-spreading mid-atlantic ridge, south of the kane transform zone (MARK), in: Proceedings of the Ocean Drilling Program, 153 Scientific Results. Ocean Drilling Program, pp. 437–456. https://doi.org/10.2973/odp.proc.sr.153.043.1997

Miller, H.M., Matter, J.M., Kelemen, P., Ellison, E.T., Conrad, M.E., Fierer, N., Ruchala, T., Tominaga, M., Templeton, A.S., 2016. Modern water/rock reactions in oman hyperalkaline peridotite aquifers and implications for microbial habitability. Geochimica et cosmochimica acta 179, 217–241. https://doi.org/10.1016/j.gca.2016.01.033

Minshull, T.A., White, R.S., 1996. Thin crust on the flanks of the slow-spreading southwest indian ridge. Geophysical Journal International 125, 139–148. https://doi.org/10.1111/j.1365-246X.1996.tb06541.x

Minshull, T.A., White, R.S., Mutter, J.C., Buhl, P., Detrick, R.S., Williams, C.A., Morris, E., 1991. Crustal structure at the blake spur fracture zone from expanding spread profiles. Journal of geophysical research 96, 9955–9984. https://doi.org/10.1029/91jb00431

Muller, M.R., Robinson, C.J., Minshull, T.A., White, R.S., Bickle, M.J., 1997. Thin crust beneath ocean drilling program borehole 735B at the southwest indian ridge? Earth and planetary science letters 148, 93–107. https://doi.org/10.1016/S0012-821X(97)00030-7

Nicolas, A., Boudier, F., Ildefonse, B., Ball, E., 2000. Accretion of oman and united arab emirates ophiolite – discussion of a new structural map. Marine Geophysical Researches 21, 147–180. https://doi.org/10.1023/A:1026769727917

Okamoto, A., Oyanagi, R., Yoshida, K., Uno, M., Shimizu, H., Satish-Kumar, M., 2021. Rupture of wet mantle wedge by self-promoting carbonation. Communications Earth & Environment 2, 1–10. https://doi.org/10.1038/s43247-021-00224-5

Okamoto, A., Shimizu, H., 2015. Contrasting fracture patterns induced by volume-increasing and -decreasing reactions: Implications for the progress of metamorphic reactions. Earth and planetary science letters 417, 9–18. https://doi.org/10.1016/j.epsl.2015.02.015

Okino, K., Matsuda, K., Christie, D.M., Nogi, Y., Koizumi, K.-I., 2004. Development of oceanic detachment and asymmetric spreading at the australian-antarctic discordance. Geochemistry, Geophysics, Geosystems 5. https://doi.org/10.1029/2004gc000793

Oufi, O., Cannat, M., Horen, H., 2002. Magnetic properties of variably serpentinized abyssal peridotites. Journal of Geophysical Research, [Solid Earth] 107, EPM 3-1-EPM 3-19. https://doi.org/10.1029/2001JB000549

Peacock, S.M., 2001. Are the lower planes of double seismic zones caused by serpentine dehydration in subducting oceanic mantle? Geology 29, 299–302. https://doi.org/10.1130/0091-7613(2001)029%3C0299:ATLPOD%3E2.0.CO;2

Plümper, O., King, H.E., Geisler, T., Liu, Y., Pabst, S., Savov, I.P., Rost, D., Zack, T., 2017. Subduction zone forearc serpentinites as incubators for deep microbial life. Proceedings of the National Academy of Sciences of the United States of America 114, 4324–4329. https://doi.org/10.1073/pnas.1612147114

Ranero, C.R., Morgan, J.P., McIntosh, K., Reichert, C., 2003. Bending-related faulting and mantle serpentinization at the middle america trench. Nature 425, 367–373. https://doi.org/10.1038/nature01961

Rioux, M., Bowring, S., Kelemen, P., Gordon, S., Dudás, F., Miller, R., 2012. Rapid crustal accretion and magma assimilation in the Oman-UAE ophiolite: High precision U-Pb zircon geochronology of the gabbroic crust. J Geophys Res [Solid Earth] 117. https://doi.org/10.1029/2012JB009273

Rouméjon, S., Cannat, M., 2014. Serpentinization of mantle-derived peridotites at mid-ocean ridges: Mesh texture development in the context of tectonic exhumation. Geochemistry, Geophysics, Geosystems 15, 2354–2379. https://doi.org/10.1002/2013gc005148

Streit, E., Kelemen, P., Eiler, J., 2012. Coexisting serpentine and quartz from carbonate-bearing serpentinized peridotite in the samail ophiolite, oman. Contributions to mineralogy and petrology. Beitrage zur Mineralogie und Petrologie 164, 821–837. https://doi.org/10.1007/s00410-012-0775-z

Takai, K., Nakamura, K., Suzuki, K., Inagaki, F., Nealson, K.H., Kumagai, H., 2006. Ultramafics-hydrothermalism-hydrogenesis-HyperSLiME (UltraH3) linkage: A key insight into early microbial ecosystem in the archean deep-sea hydrothermal systems. Paleontological Research 10, 269–282. https://doi.org/10.2517/prpsj.10.269

Toft, P.B., Arkani-Hamed, J., Haggerty, S.E., 1990. The effects of serpentinization on density and magnetic susceptibility: A petrophysical model. Physics of the Earth and Planetary Interiors 65, 137–157. https://doi.org/10.1016/0031-9201(90)90082-9

Tutolo, B.M., Mildner, D.F.R., Gagnon, C.V.L., Saar, M.O., Seyfried, W.E., 2016. Nanoscale constraints on porosity generation and fluid flow during serpentinization. Geology 44, 103–106. https://doi.org/10.1130/G37349.1

Ueki, K., Iwamori, H., 2017. Geochemical differentiation processes for arc magma of the sengan volcanic cluster, northeastern japan, constrained from principal component analysis. Lithos 290-291, 60–75. https://doi.org/10.1016/j.lithos.2017.08.001

Ulven, O.I., Jamtveit, B., Malthe-Sørenssen, A., 2014. Reaction-driven fracturing of porous rock. Journal of Geophysical Research, [Solid Earth] 119, 7473–7486. https://doi.org/10.1002/2014jb011102

Uno, M., Koyanagawa, K., Kasahara, H., Okamoto, A., Tsuchiya, N., 2022. Volatile-consuming reactions fracture rocks and self-accelerate fluid flow in the lithosphere. Proceedings of the National Academy of Sciences of the United States of America 119. https://doi.org/10.1073/pnas.2110776118

Yasukawa, K., Nakamura, K., Fujinaga, K., Iwamori, H., Kato, Y., 2016. Tracking the spatiotemporal variations of statistically independent components involving enrichment of rare-earth elements in deep-sea sediments. Scientific reports 6, 29603. https://doi.org/10.1038/srep29603

Yokoyama, T., Nakashima, S., 2005. Color development of iron oxides during rhyolite weathering over 52,000 years. Chemical geology 219, 309–320. https://doi.org/10.1016/j.chemgeo.2005.03.005

Yoshida, K., Kuwatani, T., Hirajima, T., Iwamori, H., Akaho, S., 2018. Progressive evolution of whole-rock composition during metamorphism revealed by multivariate statistical analyses. Journal of Metamorphic Geology 36, 41–54. https://doi.org/10.1111/jmg.12282

Yoshida, K., Okamoto, A., Shimizu, H., Oyanagi, R., Tsuchiya, N., Oman Drilling Project Phase 2 Science Party, 2020. Fluid infiltration through oceanic lower crust in response to reaction-induced fracturing: Insights from serpentinized troctolite and numerical models. Journal of Geophysical Research, [Solid Earth] 125. https://doi.org/10.1029/2020jb020268

Yoshida, K., Oyanagi, R., Kimura, M., Plümper, O., Fukuyama, M., Okamoto, A., 2023. Geological records of transient fluid drainage into the shallow mantle wedge. Science advances 9, eade6674. https://doi.org/10.1126/sciadv.ade6674

Supplementary materials for

Alteration processes for mantle peridotite of the Samail ophiolite revealed by independent component analysis of physical properties

Y. Akamatsu[1], T. Kuwatani[1], and R. Oyanagi[2,1]

1. Research Institute for Marine Geodynamics, Japan Agency for Marine–Earth Science and Technology (JAMSTEC), Kanagawa, Japan

2. School of Science and Engineering, Kokushikan University, Tokyo, Japan

Corresponding author: Yuya Akamatsu (akamatsuy@jamstec.go.jp)

Physical property measurements

During core description campaigns on the D/V Chikyu, the physical properties of the recovered core samples were systematically analyzed, including density, porosity, P-wave velocity, electrical resistivity, and magnetic susceptibility. These measurements were made on discrete core samples cut into ca. 2 × 2 × 2 cm cubes at laboratory temperature and pressure conditions. For a more details in each measurement, please refer to Kelemen et al. (2020). The mass and volume of the samples were determined using a dual balance system and a gas pycnometer, and grain density was calculated from the dry mass and solid volume, while porosity was determined by subtracting the wet mass from the dry mass. These density and porosity data were used for outlier detection for our dataset and the data from the remaining 194 samples were used for our analysis.

Grain density can be used to infer degree of hydration of mantle peridotite, since hydration of peridotite is accompanied primarily with alteration of olivine (3.3 g/cm^3) into serpentine (2.5 g/cm^3). Hydration degree d is empirically defined as (Miller and Christensen, 1997):

$$d = \frac{3.3 - \rho_{\mathrm{grain}}}{0.785},$$

where ρ_{grain} is grain density. Although this equation does not account for the effects of minerals other than olivine and serpentinite, and thus has some uncertainty in estimating the degree of alteration, it is useful in broadly assessing how the alteration process develops.

P-wave velocity was measured in three orthogonal directions in core samples that wre saturated with NaCl solution (3.5 g/L). The ultrasonic velocity measurements were carried out with a PWV-D system (GEOTEK) comprising P-wave transducers with a resonant frequency of 230 kHz. The first arrival was identified by the system and the velocity was determined by dividing the sample length by the travel time. System calibration runs were conducted using a series of acrylic and glass cylinders of different thicknesses. We made eight measurements in each direction of the core samples, and used an average value, which typically results in <1% variation.

The electrical resistivity was measured in three orthogonal directions using an Agilent 4294A Procession Impedance Analyzer with a set of two stainless steel electrodes. Measurements were carried at laboratory temperatures of 22.5 to 23.3°C, resulting in a temperature-induced resistivity variation of ~1%, which is broadly equivalent to the accuracy of sample dimensions. Two paper filters soaked in brine for wet measurements and two stainless steel mesh filters for dry measurements were placed between the steel electrodes and sample cube on its topside and bottomside to enhance coupling. The magnitude ($|Z|$) and phase angle (θ) of the complex impedance were measured at 25 kHz across the array from 40 Hz to 10 MHz. The resistivity was calculated from the sample impedance, length, and cross-sectional area in each orientation.

The measured dry and wet resistivities data were used for model the bulk permeability to highlight the impact of alteration on fluid transportation (Katayama et al., 2020). The transport porosity which primarily affects the rock's transport properties was first calculated from the difference between dry and wet resistivities based on the Hashin-Shtrikman bound theory (Mavko et al., 2020). Then, the bulk permeability was estimated from an empirical relationship between the transport porosity and permeability, that calibrated via direct measurements of permeability.

Bulk magnetic susceptibility was measured using an AGICO KLY-3 Kappabridge susceptibility meter or MS2B Bartington susceptibility meter after every heating step to monitor thermal alteration of magnetic minerals during heating.

In addition to the discrete physical properties, we included the color reflectance data that were measured on the half core sections during the shipboard descriptions to the multivariate analysis (Kelemen et al., 2020). The colorimetry data provide relative changes in the composition of the bulk material and are widely used to correlate sections from core to core or hole to hole and to analyze the characteristics of lithologic changes. Color reflectance was categorized as an International Oceanic Drilling Program (IODP) standard measurement, and the measured color spectrum is normally converted to L*, a*, and b* parameters. L* is lightness (greater value = lighter) in the range between 0 (black) and 100 (white), a* is the red-green value (greater value = redder) in the range between –60 (green) and 60 (red), and b* is the yellow-blue value (greater value = yellower) in the range between –60 (blue) and 60 (yellow).

References

Katayama, I., Abe, N., Hatakeyama, K., Akamatsu, Y., Okazaki, K., Ulven, O.I., Hong, G., Zhu, W., Cordonnier, B., Michibayashi, K., Godard, M., Kelemen, P., the Oman Drilling Project Phase 2 Science Party, 2020. Permeability profiles across the crust-mantle sections in the oman drilling project inferred from dry and wet resistivity data. Journal of Geophysical Research, [Solid Earth] 125. https://doi.org/10.1029/2019jb018698

Kelemen, P.B., Matter, J.M., Teagle, D.A.H., Coggon, J.A., the Oman Drilling Project Science Team, 2020. Proceedings of the oman drilling project. International Ocean Discovery Program College Station, TX.

Mavko, G., Mukerji, T., Dvorkin, J., 2020. The rock physics handbook. Cambridge University Press.

Miller, D.J., Christensen, N.I., 1997. Seismic velocities of lower crustal and upper mantle rocks from the slow-spreading Mid-Atlantic ridge, south of the kane transform zone (MARK), in: Proceedings of the Ocean Drilling Program, 153 Scientific Results. Ocean

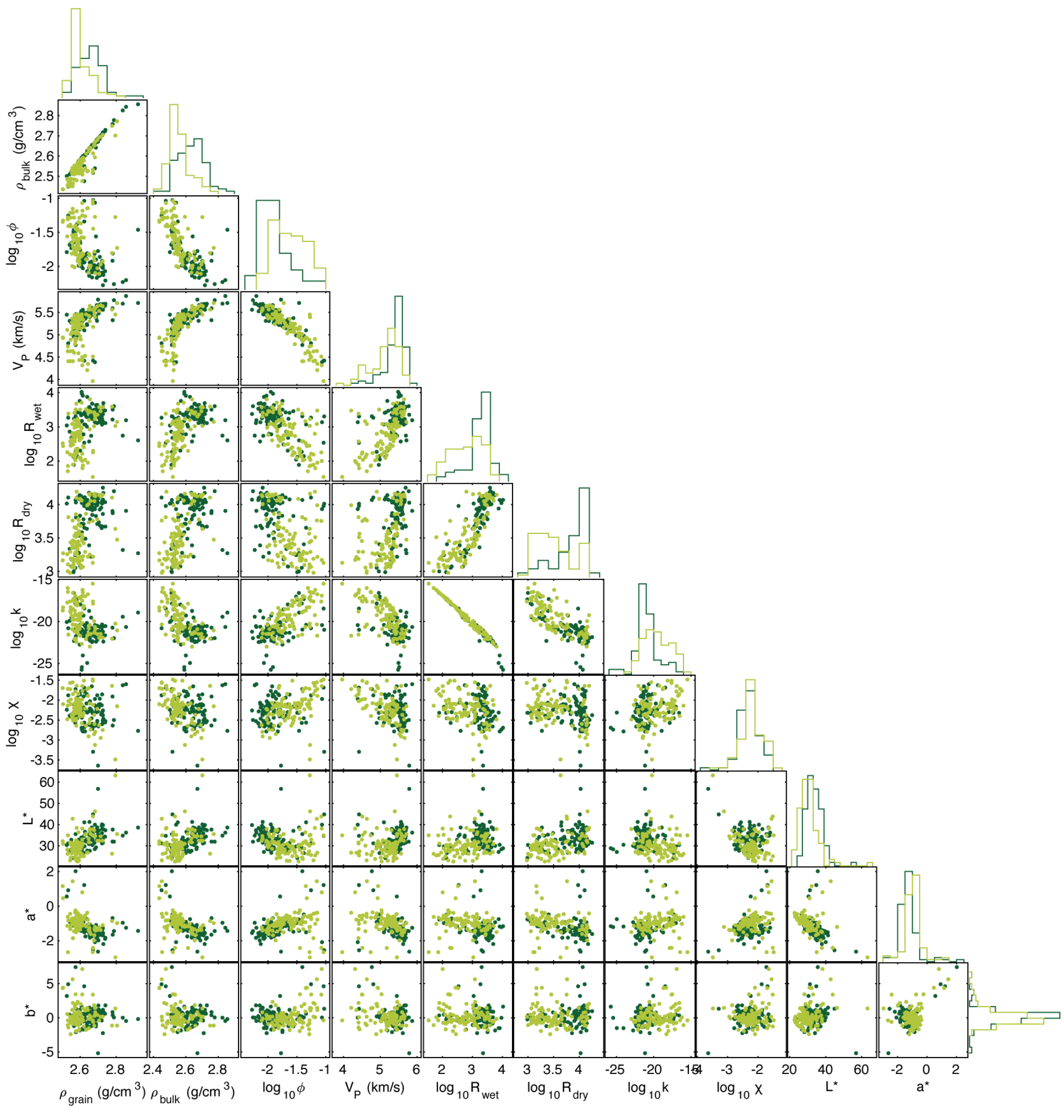

Fig. S 1 Scatter plots of the input physical properties data. Dark and light green symbols represent harzburgite and dunite samples, respectively.

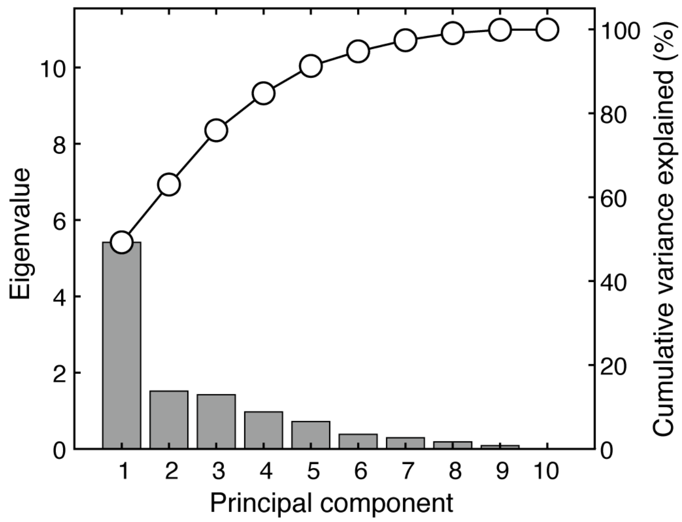

Fig. S 2 Eigenvalue of each principal component vector showing variance of data variation (bars, left axis) and cumulative propotion of the variance explained (circle symbols, right axis).

Drilling Program, pp. 437–456. https://doi.org/10.2973/odp.proc.sr.153.043.1997

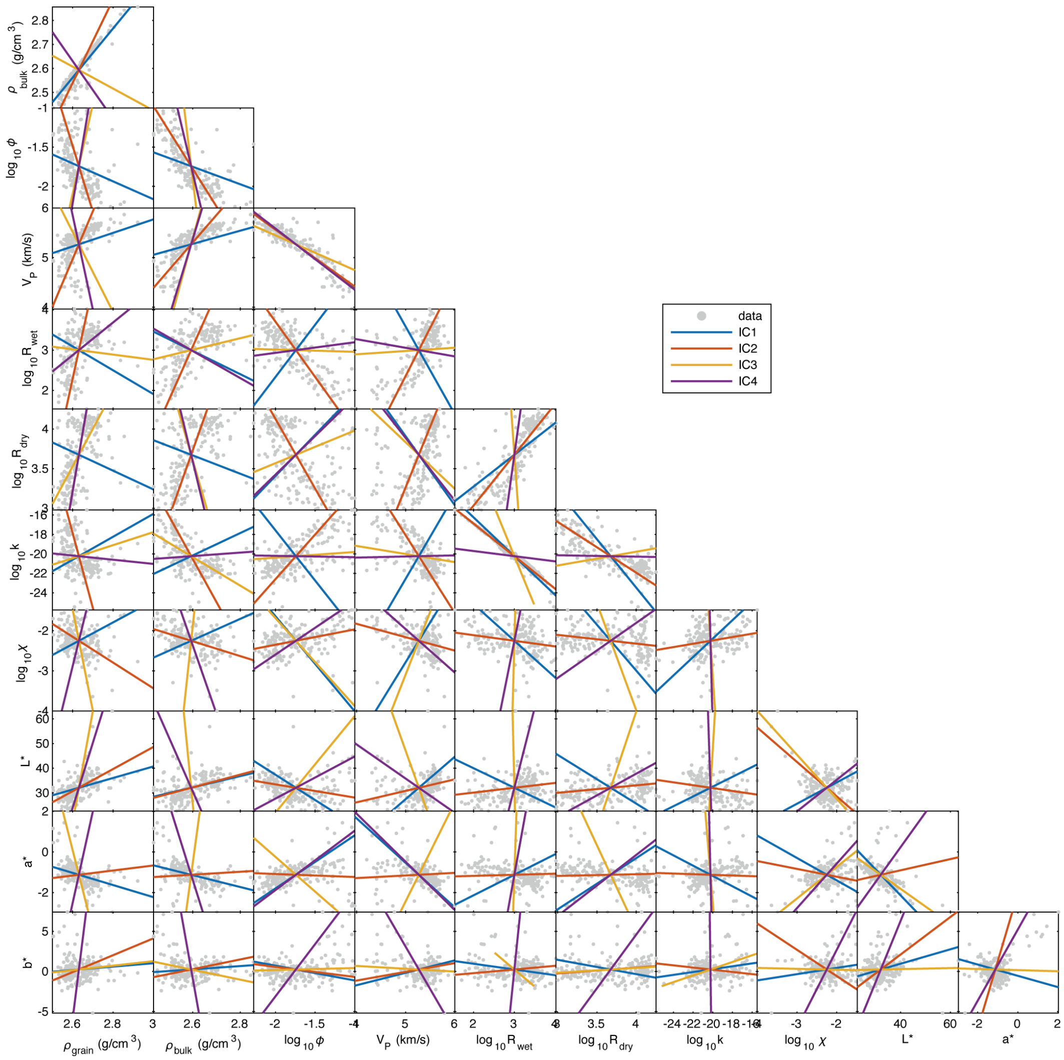

Fig. S 3 Scatter plots of the all physical properties data, plotted with independent component vectors.